JBC RESEARCH ARTICLE

# CTCF and BORIS-mediated autophagy regulation *via* alternative splicing of BNIP3L in breast cancer

Received for publication, October 18, 2023, and in revised form, May 9, 2024 Published, Papers in Press, May 27, 2024,
https://doi.org/10.1016/j.jbc.2024.107416

**Anchala Pandey, Parik Kakani, and Sanjeev Shukla***

*From the Department of Biological Sciences, Indian Institute of Science Education and Research, Bhopal, Madhya Pradesh, India*

Reviewed by members of the JBC Editorial Board. Brian D. Strahl

**Autophagy is a pivotal regulatory and catabolic process, induced under various stressful conditions, including hypoxia. However, little is known about alternative splicing of autophagy genes in the hypoxic landscape in breast cancer. Our research unravels the hitherto unreported alternative splicing of BNIP3L, a crucial hypoxia-induced autophagic gene. We showed that BNIP3L, under hypoxic condition, forms two isoforms, a full-length isoform (BNIP3L-F) and a shorter isoform lacking exon 1 (BNIP3L-Δ1). The hypoxia-induced BNIP3L-F promotes autophagy, while under normoxia, the BNIP3L-Δ1 inhibits autophagy. We discovered a novel dimension of hypoxia-mediated epigenetic modification that regulates the alternative splicing of BNIP3L. Here, we showed differential DNA methylation of BNIP3L intron 1, causing reciprocal binding of epigenetic factor CCCTC-binding factor (CTCF) and its paralog BORIS. Additionally, we highlighted the role of CTCF and BORIS impacting autophagy in breast cancer. The differential binding of CTCF and BORIS results in alternative splicing of BNIP3L forming BNIP3L-F and BNIP3L-Δ1, respectively. The binding of CTCF on unmethylated BNIP3L intron 1 under hypoxia results in RNA Pol-II pause and inclusion of exon 1, promoting BNIP3L-F and autophagy. Interestingly, the binding of BORIS on methylated BNIP3L intron 1 under normoxia also results in RNA Pol-II pause but leads to the exclusion of exon 1 from BNIP3L mRNA. Finally, we reported the critical role of BORIS-mediated RNA Pol-II pause, which subsequently recruits SRSF6, redirecting the proximal splice-site selection, promoting BNIP3L-Δ1, and inhibiting autophagy. Our study provides novel insights into the potential avenues for breast cancer therapy by targeting autophagy regulation, specifically under hypoxic condition.**

Hypoxia is considered one of the hallmarks of breast cancer (1, 2), and this unequal distribution of oxygen due to chaotic tumor organization and poor vasculature activates several stress regulatory pathways for survival, such as epithelial to mesenchymal transition (3),invasion (4), migration (5), angiogenesis (6), and autophagy (7). Macroautophagy (hereafter referred to as autophagy) is a stress adaptive response that maintains cellular integrity and concomitantly eradicates toxic molecules within autophagosomes (8). Hypoxic condition activates hypoxia-inducible factor 1 α (HIF1α) targeted autophagic genes BNIP3 and BNIP3L, which competitively bind Bcl-2 and Bcl-XL, replacing and releasing BECN1. The released BECN1 then participates in the class III phosphatidylinositol 3-kinase (PI3K-III) complex, promoting autophagosome formation and autophagy (7). The multifaceted role of autophagy in tumor development is a subject of extensive discussion (9), and recent studies have highlighted the role of autophagy as a survival mechanism in hypoxic tumor cells (10, 11). Nevertheless, the precise mechanisms governing hypoxia-induced autophagy remain relatively understudied.

Recently, epigenetics gained much importance in governing cancer progression and various hallmarks of the cancer (12). Notably, various epigenetic factors, including CTCF and BORIS, bind the target DNA sequences in a DNA methylation-dependent manner (13). Previously, we have reported the pivotal role of interaction between DNA methylation and CTCF/BORIS in governing alternative splicing regulation (6, 14–16). However, CTCF and BORIS's role in regulating alternative splicing of autophagic genes in breast cancer has not been studied before. Therefore, in this study, we further expanded our experiments to decipher the role of these epigenetic factors in regulating autophagy in breast cancer cells.

Herein, we systematically studied the role of CTCF and BORIS in linking DNA methylation with alternative splicing of autophagic genes. Our study showed that CTCF promotes autophagy in breast cancer cells under hypoxia. Furthermore, we found that BNIP3L is a novel target of CTCF regulating autophagy under hypoxia. BNIP3L mRNA undergoes alternative splicing to form the full-length isoform BNIP3L-F under hypoxic conditions, which activates autophagy. However, under normoxia, the exclusion of exon 1 from BNIP3L mRNA forms the shorter isoform BNIP3L-Δ1 that inhibits autophagy. Mechanistically, the unmethylated BNIP3L intron 1 promotes CTCF binding and BNIP3L-F isoform under hypoxia. The enrichment of CTCF on BNIP3L intron 1 under hypoxia causes stalling of RNA Pol II, which promotes the selection of the proximal splice site and retention of the exon 1 in BNIP3L mRNA.

We also uncovered the mechanism for the exclusion of exon 1 from BNIP3L mRNA (BNIP3L-Δ1) under normoxia. Our findings indicate that BORIS, a paralog of CTCF, binds to methylated BNIP3L intron 1 under normoxia. Additionally, we

* For correspondence: Sanjeev Shukla, sanjeevs@iiserb.ac.in.

demonstrate that the binding of BORIS on BNIP3L intron 1 promotes the exon 1 exclusion and BNIP3L-Δ1. The SpliceAid revealed the binding of SRSF6 at the 5′UTR of BNIP3L mRNA under normoxia. Moreover, the decrease in pull down of SRSF6 in BORIS-depleted breast cancer cells revealed a novel mechanism of BORIS-mediated alternative splicing. Our findings indicated that the binding of BORIS recruits SRSF6 at 5′UTR of BNIP3L mRNA, redirecting the splice site selection and resulting in the exclusion of exon 1. Notably, BORIS and SRSF6 mediated exclusion of exon 1 from BNIP3L mRNA (BNIP3L-Δ1) inhibits autophagy. Consequently, the interplay between BORIS and CTCF occupancy orchestrated by hypoxia-dependent methylation at intron 1 promotes the alternative splicing of BNIP3L and facilitates the hypoxia-driven autophagy in breast cancer.

## Results

### CTCF promotes hypoxia-induced autophagy

First, we investigated the hypoxia-mediated regulation of autophagy in MCF7 and HCC1806 breast cancer cell lines. To achieve this, we analyzed the induction of autophagy under hypoxia at different time points using a common marker for autophagy turnover, examining the conversion of nonlipidated microtubule-associated protein 1A/1B light chain 3B (LC3B)-I form to lipidated LC3B-II form (10, 17) and found a hypoxia-mediated increase in LC3B-II/LC3B-I ratio under hypoxia relative to the normoxia. We further validated these findings by quantifying the autophagy receptor sequestosome1 (Sqstm1) (10) or p62 expression and observed p62 degradation under hypoxia as compared to normoxia (Fig. 1, *A* and *B*). Next, we also detected autophagic flux by enhanced GFP (EGFP)-LC3 reporter assay to monitor the formation of GFP-tagged LC3-positive autophagosomes seen as puncta (18) in control and hypoxia-treated cells. We observed an increase in the number of puncta formation of LC3-GFP fusion protein per cell under hypoxia relative to the normoxia (Fig. 1*C*). Together, we conclude that autophagy is induced under hypoxia in breast cancer cell lines corroborating with previous reports (19). As stated in the introduction, here, we investigated the role of epigenetic factors, CTCF, and BORIS in regulating autophagy. First, to evaluate the role of CTCF in autophagy regulation, we used EGFP-LC3 reporter assay in control and CTCF-depleted breast cancer cells (Fig. 1*D*). We observed a nonsignificant change in LC3-GFP puncta in CTCF-depleted cells under normoxia as compared to control normoxic cells. However, the significant increase in the number of LC3-GFP puncta from normoxia to hypoxia in control cells was attenuated in CTCF-depleted cells under hypoxia (Fig. 1*E*). We further confirm autophagy activity through immunoblotting by comparing the LC3B-II/LC3B-I ratio between control and CTCF-depleted cells under both normoxic and hypoxic conditions. Since, the autophagosomes formed during autophagy further fuse with lysosomes, forming autolysosomes that degrade sequestered cytosolic components, including LC3. We treated the cells with a lysosomal inhibitor, bafilomycin A1 (taken as positive control), that prevents the fusion of autophagosomes with lysosomes and accumulates mature autophagosomes (20). We observed that LC3B-II/LC3B-I in control cells was increased by bafilomycin A1 treatment under both normoxic and hypoxic conditions. However, CTCF knockdown cells only under hypoxia showed a decrease in the LC3B-II/LC3B-I ratio in both bafilomycin A1 treated and untreated cells as compared to the control cells. These observations indicated that the decrease in LC3B-II/LC3B-I ratio is solely attributed to CTCF depletion under hypoxia (Fig. 1, *F* and *G*) rather than degradation of LC3B-II in autolysosomes.

Furthermore, we used the mRFP-EGFP-LC3 reporter assay to analyze the formation of autophagosomes under hypoxia simultaneously with the extent of autophagic flux. As autophagosomes are formed, mRFP-EGFP-LC3 conjugates with the autophagosome membrane and is seen as yellow puncta resulting from the fluorescence of both mRFP and EGFP (Fig. 1*H*). Furthermore, when a lysosome fuses with an autophagosome to form an autolysosome, only red puncta is observed, as the fluorescent activity of EGFP is quenched in an acidic environment (18). Consecutively, CTCF depletion under hypoxia attenuated the number of both red (autolysosomes) and yellow (autophagosomes) puncta as compared to control cells under hypoxia (Fig. 1*I*). Therefore, these results indicate that CTCF deficiency impairs the autophagosome formation and autophagy under hypoxia.

### Hypoxia-induced alternative splicing of BNIP3L

CTCF's role has been examined in regulating alternative splicing of various genes, including cluster of differentiation 45 (15), and vascular endothelial growth factor A-165 (6). However, its role has not been studied in the regulation of alternative splicing of autophagic genes. To examine the role of CTCF in the regulation of autophagy at the transcriptional level under hypoxia, we collected the Gene Ontology Biological Process-positive autophagy regulatory genes list (MsigDB) followed by comparing it with hypoxia hallmark genes list (MsigDB) (21) to extract the overlapping genes (Fig. 2*A*). We collected total nine overlapping genes and specifically focused on BNIP3L that plays a crucial role in mitophagy and macroautophagy (7, 22). Additionally, Bellot *et al.* also reported BNIP3L's role in hypoxia-induced autophagy (7). Moreover, a recent report mentioned the existence of two isoforms of the BNIP3L that differ in exon 1 (23). However, the molecular mechanism governing the alternative splicing and significance of each isoform in the regulation of autophagy has not been discussed before.

From our study, we observed BNIP3L pre-mRNA undergoes alternative splicing to form two isoforms carrying a difference of exon 1, and accordingly named the full-length isoform as BNIP3L-F and the shorter isoform lacking exon 1 as BNIP3L-Δ1 (Fig. 2*B*). To further validate the expression of each isoform under hypoxia in breast cancer cell lines, we prepared exon specific primers and performed a semi-quantitative PCR (semi-qPCR) analysis in normoxic *versus* hypoxic MCF7 and HCC1806 cells (Fig. 2*C*). Furthermore, we performed quantitative reverse transcription PCR (qRT-PCR) analysis at different time points in normoxic *versus* hypoxic MCF7 and

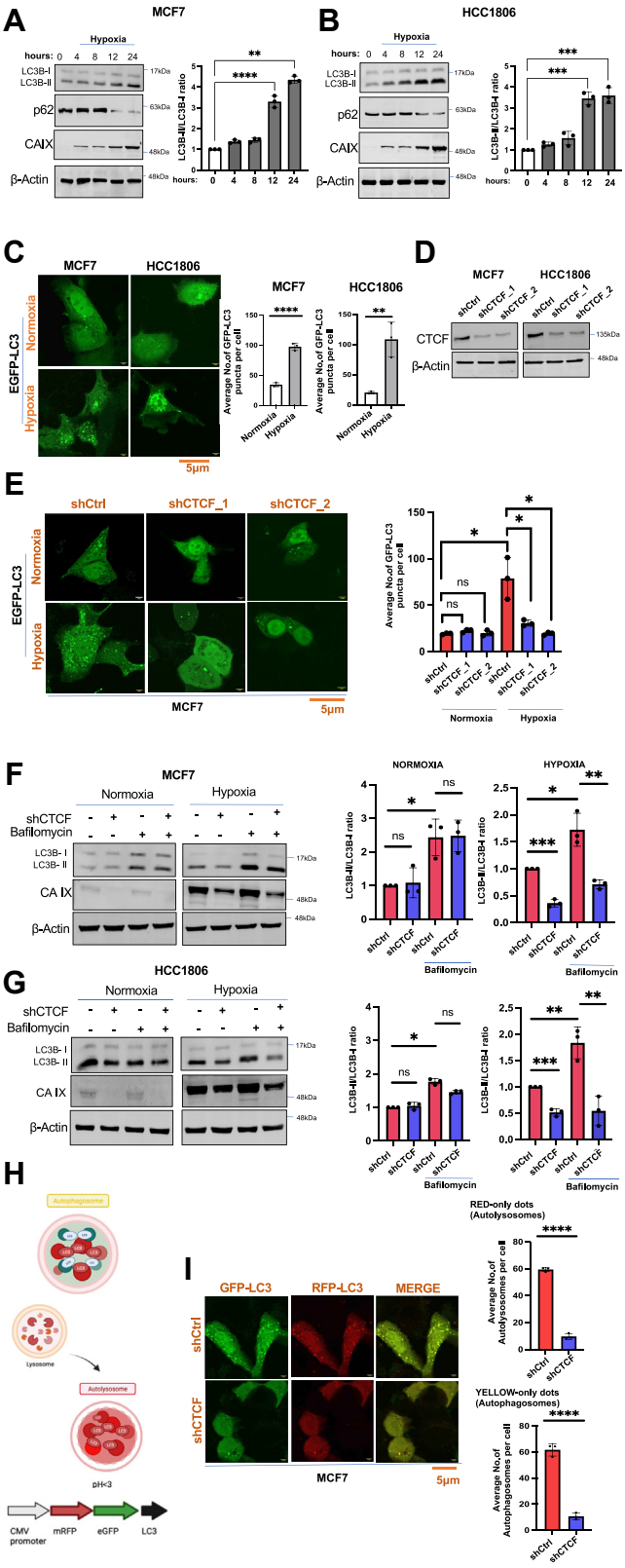


**Figure 1. CTCF promotes hypoxia-induced autophagy.** *A* and *B*, immunoblots for hypoxia-treated cells at different time points measuring microtubule associated protein 1A/1B light chain 3B (LC3B)-II/LC3B-I ratio, p62, and CAIX expression in (*A*) MCF7 and (*B*) HCC1806 cells. Graph showing the average of three independent experiments measuring LC3B-II/LC3B-I ratio. *C*, MCF7 and HCC1806 cells transfected with EGFP-LC3 plasmid and incubated in hypoxia (1% oxygen) for 12 h. LC3–GFP puncta analyzed. The scale bar represents 5 μm. Data represent the mean ± SD from three independent experiments. *D*, immunoblots measuring CTCF expression in CTCF knockdown MCF7 and HCC1806 cells. *E*, CTCF knockdown MCF7 cells were transfected with EGFP-LC3 plasmid, and cells incubated in hypoxia (1% oxygen) for 12 h. LC3–GFP puncta were analyzed. The scale bar represents 5 μm. Data represent the mean ± SD from three independent experiments. *F* and *G*, immunoblots for measuring LC3B-II/LC3B-I ratio, CAIX in CTCF knockdown treated in normoxic *versus* hypoxic condition for 12 h (*F*) MCF7 cells and (*G*) HCC1806 cells. Graph showing the average of three independent experiments measuring LC3B-II/LC3B-I ratio. The same cells were treated with bafilomycin and were taken as a positive control. *H*, pictorial representation of the mechanism of ptf-LC3 plasmid. *I*, ptf-LC3 plasmid (Cat#21074) transfected in CTCF knockdown MCF7 cells. The scale bar represents 5 μm. Average number of autophagosomes (*yellow* only dots) and autolysosomes (*red* only dots) in three independent experiments. Data represent the mean ± SD from three independent experiments. Statistical significance was determined using unpaired Student's t test (*$p < 0.05$, **$p < 0.01$, ***$p < 0.001$, and ****$p < 0.0001$, while a lack of significance is represented by "ns" for $p > 0.05$). Error bars show mean values ± SD (n = 3 unless otherwise specified).

HCC1806 cells (Fig. S1, *A* and *B*). The analysis revealed an increase in the expression of the BNIP3L-F isoform while a substantial decrease in the BNIP3L-Δ1 isoform under hypoxia relative to control normoxia (Figs. 2*D* and S1, *A* and *B*). The two fragments were gel extracted and confirmed by Sanger sequencing, as shown in Figure 2*E*. To assess the expression level of each isoform at the protein level, we conducted immunoblot analyses of normoxic *versus* hypoxic breast cancer cells indicating an increase in expression of BNIP3L-F, and a decrease in expression of BNIP3L-Δ1 under hypoxia as mentioned in Figure 2*F*. Next, we wanted to decipher the role of each isoform in regulating autophagy under hypoxia. For this, we overexpressed the two isoforms individually in BNIP3L knockdown cells (endogenous BNIP3L depletion) and analyzed the change in the autophagy by monitoring the LC3B-II/LC3B-I ratio. The overexpression of BNIP3L-F isoform increased the LC3B-II/LC3B-I ratio and, hence, autophagy in BNIP3L knockdown normoxic MCF7 cells (Fig. 2*G*). Moreover, the overexpression of the BNIP3L-Δ1 isoform in BNIP3L-depleted cells attenuated autophagy in normoxic MCF7 cells. Similar results were obtained when we checked the formation of autophagosomes and observed an increased number of GFP-LC3 puncta per cell upon BNIP3L-F overexpression in BNIP3L-depleted normoxic MCF7 cells (Fig. 2*H*). These results indicated that the BNIP3L-F isoform promotes autophagy while the BNIP3L-Δ1 isoform inhibits autophagy.

Several reports showed that BNIP3L binds Bcl-2 under hypoxia to promote autophagy (7). The binding of BNIP3L replaces BECN1 from the Bcl-2-BECN1 complex, thereby allowing the released BECN1 to further promote the autophagosome formation (24). To speculate the particular isoform of BNIP3L that interacts with Bcl-2 to displace BECN1, we performed a coimmunoprecipitation (Co-IP) assay. The assay was conducted using BNIP3L-depleted MCF7 cell lysates, with exogenously expressing both Flag-tagged BNIP3L isoforms individually (Fig. 2*J*). In Flag pull-down, the interaction of BNIP3L-F is relatively more with Bcl-2 than BNIP3L-Δ1. Furthermore, the overexpression of BNIP3L-Δ1 had no effect on the interaction of Bcl-2 and BECN1. In the pull down of Bcl-2, BECN1 showed interaction with Bcl-2 in exogenously expressed BNIP3L-Δ1 MCF7 cell lysate. Similarly, in the pull down of BECN1, Bcl-2 showed interaction with BECN1 in

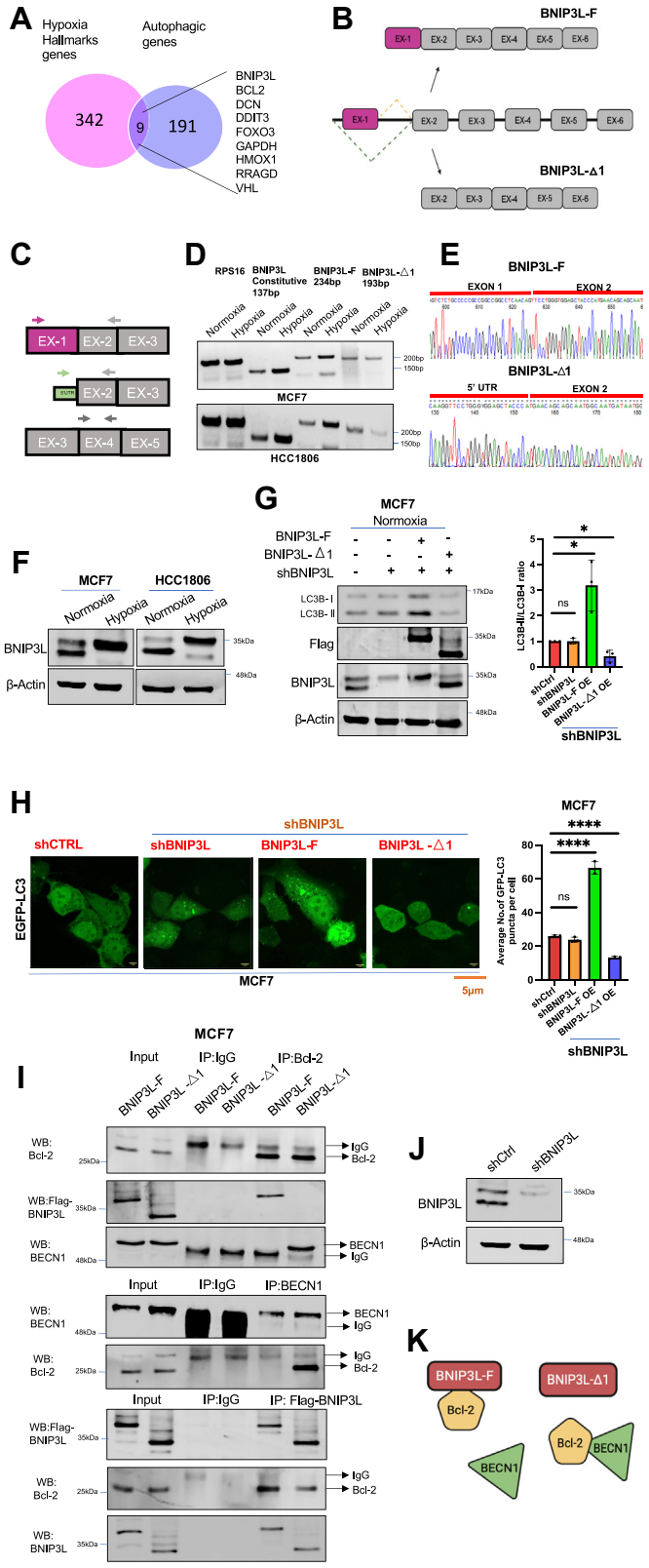


**Figure 2. Hypoxia-induced alternative splicing of BNIP3L.** *A*, Venn diagram representing a total of nine overlapped genes from hypoxia hallmark genes list and GOBP positive autophagy regulatory genes list (MSigDB). *B*, schematic diagram showing the two isoforms and alternative splicing of BNIP3L (*pink*-exon 1 and *gray*-constitutive exon). *C*, schematic representing three primers designed for semi-qPCR. *D*, semi-qPCR performed in MCF7 and HCC1806 cells with isoform-specific primers measuring expression of each isoform treated under hypoxia for 12 h. *E*, the results of Sanger sequencing of the BNIP3L-F and BNIP3L-Δ1 isoforms purified from corresponding gels. *F*, immunoblots measuring BNIP3L expression in normoxic *versus* hypoxic condition (12 h) in MCF7 and HCC1806 cells. *G*, immunoblots measuring LC3B-II/LC3B-I ratio, Flag, and BNIP3L expression in exogenously expressed Flag-tag BNI3PL-F and Flag-tag BNIP3L-Δ1 in endogenously depleted BNIP3L MCF7 cells. Graph showing the average of three independent experiments measuring LC3B-II/LC3B-I ratio. *H*, same cells transfected with EGFP-LC3 plasmid and were incubated in hypoxia (1% oxygen). LC3–GFP puncta analyzed. The scale bar represents 5 μm. Data represent the mean ± SD from three independent experiments. *I*, coimmunoprecipitation performed in MCF7 cell lysate. The immunoprecipitated samples were analyzed by immunoblotting using anti-Bcl-2, anti-BNIP3L, anti-Flag, and anti-BECN1 antibodies. *J*, immunoblots representing expression of BNIP3L in BNIP3L knockdown MCF7 cells. *K*, schematic representing the interaction of BNIP3L isoform with Bcl-2-BECN1 complex. Data represent the mean ± SD from three independent experiments. Statistical significance was determined using unpaired Student's t test (*$p < 0.05$, **$p < 0.01$, ***$p < 0.001$, and ****$p < 0.0001$, while a lack of significance is represented by "ns" for $p > 0.05$). Error bars show mean values ± SD (n = 3 unless otherwise specified).

exogenously expressed BNIP3L-Δ1 MCF7 cell lysate (Fig. 2*I*). These findings suggest that BNIP3L-F exhibits a higher affinity for Bcl-2 compared to BNIP3L-Δ1, consequently displacing BECN1 from the Bcl-2-BECN1 complex (Fig. 2*K*). Thereby, these results demonstrate that the hypoxic isoform BNIP3L-F promotes autophagy, while normoxic isoform BNIP3L-Δ1 inhibits autophagy.

### *CTCF promotes BNIP3L-F isoform by favoring the inclusion of exon 1 in BNIP3L mRNA under hypoxia*

So far, we have deciphered the involvement of CTCF in the positive regulation of autophagy under hypoxia. Additionally, we deciphered hypoxia-mediated alternative splicing of BNIP3L, forming two isoforms. Our next objective was to decipher the molecular mechanism governing the alternative splicing of BNIP3L under hypoxia. Previous reports suggested the intragenic role of CTCF that links DNA methylation with alternative splicing (15, 16). The binding of CTCF to its DNA sites creates a roadblock to the transcriptional elongation due to RNA Pol II pause and results in the inclusion of the alternate exon. However, intragenic DNA methylation releases RNA Pol II from its transient blockage by inhibiting the binding of CTCF and promoting the exclusion of the alternative exon (15). Altogether, considering the CTCF involvement in alternative splicing by causing Pol II pause (15) and alternative splicing of BNIP3L exon 1, we hypothesized that CTCF might promote the BNIP3L alternative splicing under hypoxia and hence autophagy. Interestingly, using chromatin immunoprecipitation (ChIP) atlas, we observed a novel potential binding of CTCF on BNIP3L intron 1 in breast cancer cell lines (Fig. 3*A*). Considering this observation, we first used methylated DNA immunoprecipitation (MeDIP)-qPCR to check the methylation levels of BNIP3L intron 1 at the CTCF binding site (Fig. 3*A*) in normoxia *versus* different time points of hypoxia-treated breast cancer cells. We observed DNA demethylation on BNIP3L intron 1 under hypoxic relative to control normoxic MCF7 (Fig. 3*B*) and HCC1806 cells (Fig. S2*A*). We further performed MeDIP-qPCR using H19 imprinting control region primers (25). Here, H19 imprinting control region is taken as a positive control for MeDIP-qPCR

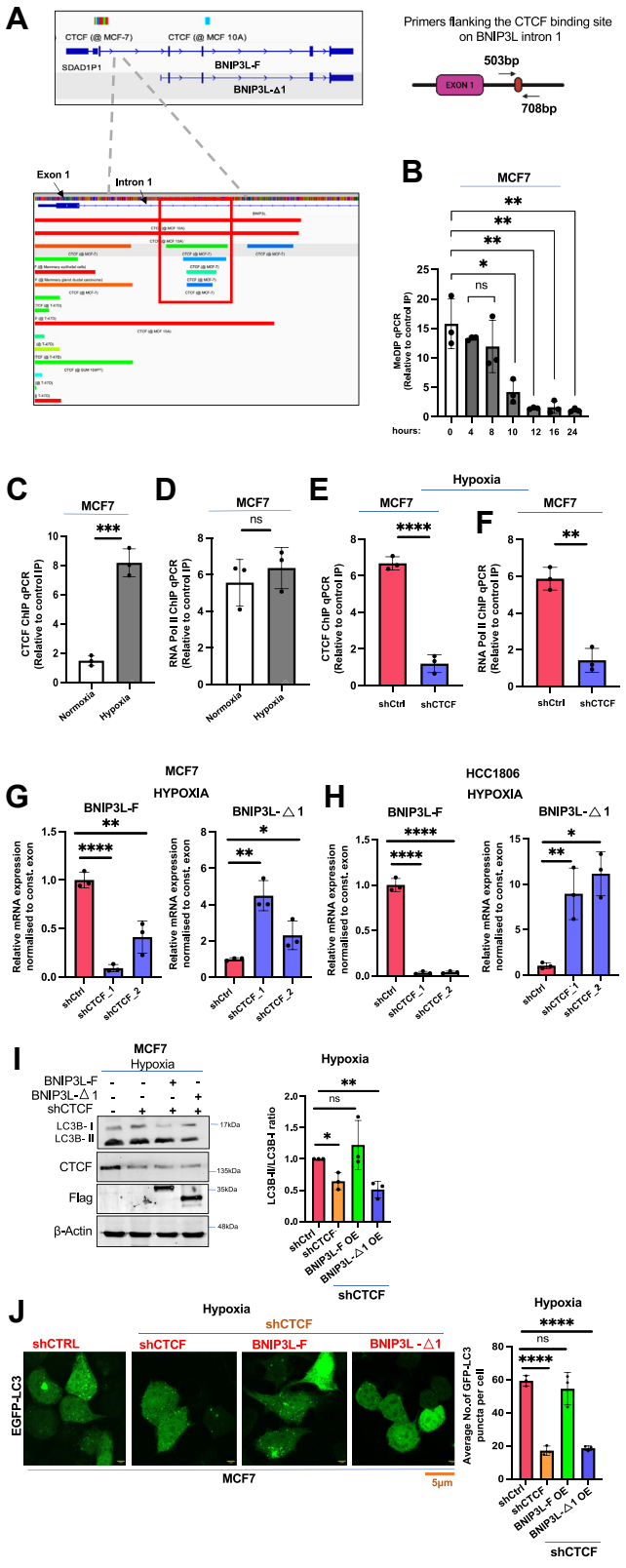


**Figure 3. CTCF promotes hypoxia-induced-autophagy by alternative splicing of BNIP3L.** *A*, ChIP atlas showing enrichment of CTCF on BNIP3L intron 1. Schematic showing primers spanning the binding site of CTCF on intron 1. *B*, MeDIP performed on BNIP3L intron 1 in MCF7 cells, incubated at different time points in hypoxic condition. *C* and *D*, ChIP of (*C*) CTCF (*D*) RNA Pol II performed on BNIP3L intron 1 with the same primers in MCF7 cells, incubated in hypoxia for 12 h. *E* and *F*, ChIP of (*E*) CTCF and (*F*) RNA Pol II performed on BNIP3L intron 1 in CTCF knockdown MCF7 cells, incubated in hypoxia (12 h). *G* and *H*, BNIP3L isoforms (BNIP3L-F and BNIP3L-Δ1) expression measured by qPCR in CTCF knockdown (*G*) MCF7 and (*H*) HCC1806 cells under hypoxia (12 h). *I*, immunoblot of CTCF knockdown cells exogenously expressed with Flag-tag BNI3PL-F and Flag-tag BNIP3L-Δ1 measuring expression of LC3B-II/LC3B-I ratio, Flag, CTCF in MCF7 cells. Graph showing the average of three independent experiments measuring LC3B-II/LC3B-I ratio. *J*, same cells transfected with EGFP-LC3 and incubated in hypoxia (1% oxygen) for 12 h. LC3–GFP puncta analyzed. The scale bar represents 5 μm. Data represent the mean ± SD from three independent experiments. Statistical significance was determined using unpaired Student's t test (*$p < 0.05$, **$p < 0.01$, ***$p < 0.001$, and ****$p < 0.0001$, while a lack of significance is represented by "ns" for $p > 0.05$). Error bars show mean values ± SD (n = 3 unless otherwise specified). ChIP, chromatin immunoprecipitation; MeDIP, methylated DNA immunoprecipitation.

(Fig. S2*B*). Further, ChIP-qPCR analyses of CTCF on BNIP3L intron 1 showed more enrichment of CTCF in hypoxic relative to normoxic MCF7 (Fig. 3*C*) and HCC1806 cells (Fig. S2*C*). Next, we inspected RNA Pol II pause in normoxic *versus* hypoxic MCF7 (Fig. 3*D*) and HCC1806 cells (Fig. S2*D*) and observed a nonsignificant change in the occupancy of RNA Pol II on intron 1. However, the occupancy of RNA Pol II gets reduced with depletion of CTCF under hypoxia as compared to control hypoxic MCF7 (Fig. 3, *E* and *F*) and HCC1806 cells (Fig. S1, *E* and *F*). More importantly, the qRT-PCR analyses comparing control and CTCF knockdown cells under hypoxic conditions showed a decrease in the expression of BNIP3L-F, while the expression of BNIP3L-Δ1 increased with CTCF depletion, when normalized to the constitutive exon (present in both isoforms) of BNIP3L mRNA (Fig. 3, *G* and *H*). Thereby, we concluded that the binding of CTCF on BNIP3L intron 1 results in stalling of RNA Pol II downstream of exon 1 that promotes exon 1 inclusion under hypoxia (BNIP3L-F).

Next, to decipher autophagy regulation by each isoform, we prepared shRNA-mediated knockdown of CTCF (Fig. 1*D*) and overexpressed both Flag-tag BNIP3L isoform individually in CTCF-depleted MCF7 cells (Fig. 3*I*). We observed a decrease in autophagy in both CTCF-depleted cell and cells expressing exogenous BNIP3L-Δ1 in CTCF-depleted cells compared to control hypoxic cells. However, autophagy was rescued by an increase in the LC3B-II/LC3B-I ratio and the number of LC3-GFP puncta upon exogenous expression of BNIP3L-F in CTCF-depleted cells (Fig. 3, *I* and *J*). Similarly, we also observed an increase in autophagy by exogenously expressing BNIP3L-F in CTCF knockdown cells under normoxia. However, autophagy gets attenuated by exogenously expressing BNIP3L-Δ1 as compared to control normoxic MCF7 cells (Fig. S2*G*).

Therefore, CTCF is significant in regulating autophagy due to its binding on BNIP3L intron 1 under hypoxia. The binding results in RNA Pol II pause and selection of 5′ splice site that promotes the inclusion of exon 1 and BNIP3L-F isoform. The BNIP3L-F is responsible for inducing autophagy in response to hypoxia. However, the regulation of BNIP3L-Δ1 and its function in inhibiting hypoxia-induced autophagy is still unclear.

### *BORIS forms BNIP3L-Δ1 under normoxia by favoring the exclusion of exon 1 in BNIP3L mRNA*

Since we observed a nonsignificant change in RNA Pol II occupancy on intron 1 under hypoxia in comparison to the

normoxia treated breast cancer cells (Fig. 3*D*), we further investigated the cause of RNA Pol II pause in normoxia and the function it is serving under normoxia. From the literature, we found that the CTCF motif can also be occupied by its paralog, BORIS. Moreover, unlike CTCF, BORIS can also bind to methylated DNA (26). Previously, our lab showed that BORIS binds to methylated DNA and causes RNA Pol II pause that affects the outcome of PKM alternative splicing in breast cancer (14). So, we further delineate whether BORIS is responsible for RNA Pol II pause and its impact on the alternative splicing of BNIP3L under normoxia. To validate the role of BORIS in alternative splicing of BNIP3L under normoxia, we first performed BORIS-ChIP-qPCR to examine the binding of BORIS on BNIP3L intron 1 under normoxic *versus* hypoxic breast cancer cells. We observed that enrichment of BORIS was more in normoxic relative to hypoxic MCF7 (Fig. 4*A*) and HCC1806 cells (Fig. S3*A*). Next, we assessed the RNA Pol II pause in control *versus* BORIS knockdown MCF7 (Fig. 4, *B* and *C*) and HCC1806 cells (Fig. S3, *B* and *C*) under normoxia by RNA Pol II-ChIP-qPCR and again observed a nonsignificant change in occupancy of RNA Pol II on intron 1. Surprisingly, we observed that as compared to control MCF7 cells (Fig. 4*D*) and HCC1806 cells (Fig. S3*D*), the occupancy of CTCF was higher in BORIS knockdown cells under normoxia. To further investigate the enrichment of CTCF in BORIS knockdown cells on BNIP3L intron 1 under normoxia, we performed MeDIP-qPCR to analyze the methylation level in BORIS depleted MCF7 (Fig. 4*B*) and HCC1806 (Fig. S3*B*) cells under normoxia. We observed DNA demethylation with BORIS depletion as compared to control MCF7 (Fig. 4*E*) and HCC1806 cells (Fig. S3*E*) under normoxia that indicated BORIS-associated methylation on BNIP3L intron 1 under normoxia.

Next, we sought to examine the significance of the BORIS's binding on the transcriptional regulation of each isoform. The qRT-PCR analyses in control *versus* BORIS knockdown cells (Fig. 6*A*) under normoxia showed a decrease in BNIP3L-Δ1 expression, while an increase in BNIP3L-F expression was noticed after normalizing it with a BNIP3L constitutive exon (Fig. 4, *F* and *G*). Therefore, we concluded that the binding of BORIS on BNIP3L intron 1 under normoxia promotes the exclusion of exon 1 in BNIP3L mRNA, forming BNIP3L-Δ1.

Furthermore, we examined the expression of BORIS by immunoblotting and observed a notable decrease in BORIS expression under hypoxia (Fig. 4*H*). These results indicated that under normoxia, the binding of BORIS on methylated DNA sequences of BNIP3L intron 1 results in the formation of BNIP3L-Δ1. However, the mechanism behind BORIS-mediated RNA Pol II pause promoting exclusion of exon 1 and formation of BNIP3L-Δ1 still needed further investigation.

### *BORIS recruits SRSF6, resulting in the exclusion of exon 1 in BNIP3L mRNA under normoxia*

To address how BORIS binding on methylated BNIP3L intron 1 results in the exclusion of exon 1, we screened the binding of different splicing factors using SpliceAid on BNIP3L 5′UTR (Fig. 5*A*) and exon 1 and observed the binding of SRSF6 on 5′UTR of BNIP3L (Fig. 5*B*). Previous studies reported a hypoxia-mediated reduction in SRSF6 expression (27), and hence we further went ahead with SRSF6 to analyze its role in the alternative splicing of BNIP3L. First, we checked the expression of SRSF6 along with BORIS in normoxia *versus* hypoxia at different time points and observed gradual down-regulation of SRSF6 expression under hypoxic condition (Fig. 5*C*). Previous studies have shown the role of SRSF6 in alternative splicing, including exon skipping of few genes (28). Taking these observations into account, we asked whether BORIS binding to BNIP3L intron 1 recruits SRSF6, which results in the exclusion of exon 1 from BNIP3L mRNA under normoxia. To test this hypothesis, we first investigated the interaction of SRSF6 with BORIS. Our coimmunoprecipitation analyses showed the interaction of SRSF6 with BORIS in MCF7 cell lysate (Fig. 5*D*). Further, in order to decipher, whether the interaction of BORIS-SRSF6 is independent of CTCF under normoxia, we analyzed the interaction of SRSF6 with CTCF in MCF7 cell lysate by coimmunoprecipitation and observed negligible interaction between them (Fig. S4*A*). After demonstrating the interaction of BORIS and SRSF6 (Fig. 5*D*), we also investigated the BORIS-mediated recruitment of SRSF6 on BNIP3L mRNA using RNA-immunoprecipitation (RNA-IP) assay in MCF7 cells. This revealed higher enrichment of SRSF6 in control cells, which significantly decreased with BORIS depletion (Fig. 5*E*). Furthermore, we examined the transcriptional regulation of both the isoforms of BNIP3L by qRT-PCR analyses in the SRSF6 knockdown cells (Fig. S4, *B–D*) and observed that after normalizing with BNIP3L constitutive exon, SRSF6 deficient cells showed an increase in expression of BNIP3L-F and a decrease in expression of BNIP3L-Δ1 (Fig. 5, *F* and *G*). Thereby, BORIS, with the aid of SRSF6, results in the exclusion of exon 1 by redirecting the splice site selection and stabilization of the BNIP3L-Δ1 isoform under normoxic condition.

### *BORIS inhibits hypoxia-induced autophagy*

Till now, we investigated that BORIS promoted BNIP3L-Δ1 expression by facilitating the binding of SRSF6 at BNIP3L mRNA under normoxia (Fig. 5, *B–E*). Additionally, BNIP3L-Δ1 is involved in the inhibition of autophagy (Fig. 2, *G–I*). Based on the above results, we next speculated whether BORIS also promotes inhibition of autophagy. To commence our investigation, we checked autophagy in BORIS knockdown cells (Fig. 6*A*) and observed a gradual increase in the number of LC3-GFP puncta (Fig. 6*B*) and LC3B-II/LC3B-I ratio (Fig. 6, *C* and *D*) in BORIS knockdown cells relative to control cells under normoxia. Similarly, we also confirmed an increase in the LC3B-II/LC3B-I ratio in bafilomycin-treated BORIS knockdown cells under normoxia (Fig. 6, *C* and *D*) as compared to bafilomycin-treated control cells. To further decipher the impact of BORIS in autophagy flux, we transfected the BORIS knockdown and control cells with tandem mRFP-EGFP-LC3 reporter plasmid. Together, the increase in

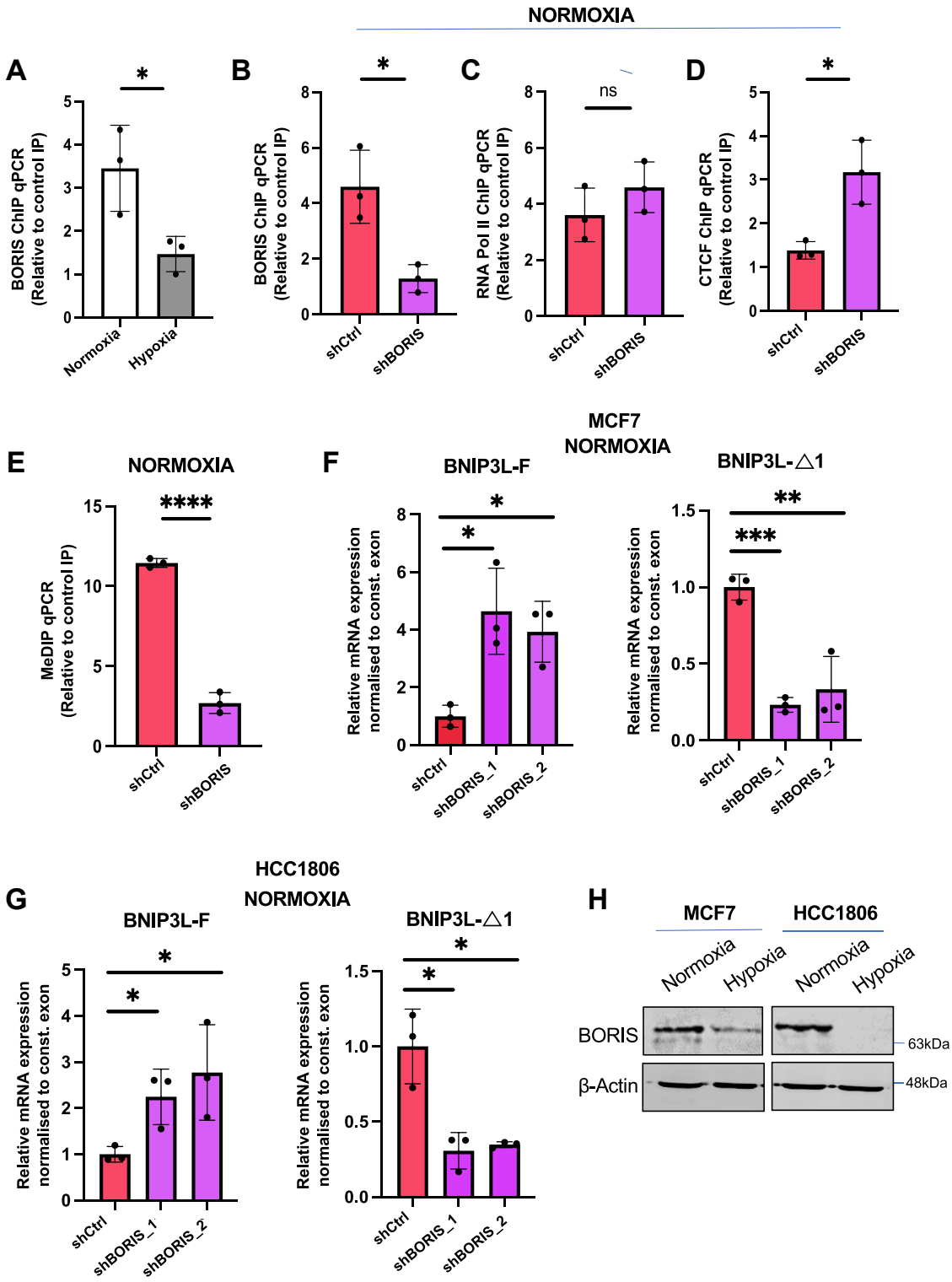


**Figure 4. BORIS forms BNIP3L-Δ1 under normoxia by favoring the exclusion of exon 1 in BNIP3L mRNA.** *A*, ChIP of BORIS performed on BNIP3L intron 1 with the same set of primers in MCF7 cells, incubated in hypoxia for 12 h. *B–D*, ChIP of (*B*) BORIS (*C*) RNA Pol II and (*D*) CTCF performed on BNIP3L intron 1 in BORIS knockdown MCF7 cells. *E*, MeDIP performed on BNIP3L intron 1 in BORIS knockdown MCF7 cells. *F* and *G*, BNIP3L isoforms expression measured by qPCR in BORIS knockdown (*F*) MCF7 and (*G*) HCC1806 cells. *H*, immunoblot measuring BORIS expression in hypoxia (12 h) treated MCF7 and HCC1806 cells. Data represent the mean ± SD from three independent experiments. Statistical significance was determined using unpaired Student's t test (*$p < 0.05$, **$p < 0.01$, ***$p < 0.001$, and ****$p < 0.0001$, while a lack of significance is represented by "ns" for $p > 0.05$). Error bars show mean values ± SD (n = 3 unless otherwise specified). MeDIP, methylated DNA immunoprecipitation.

red only (autolysosomes) and yellow only dots (autophagosomes) indicated that BORIS impedes autophagosome formation and autophagy (Fig. 6*E*).

Since we observed a decrease in BORIS expression under hypoxia (Figs. 4*H* and 5*C*) and BORIS-associated methylation on BNIP3L intron 1 under normoxia (Fig. 4*E*); we further

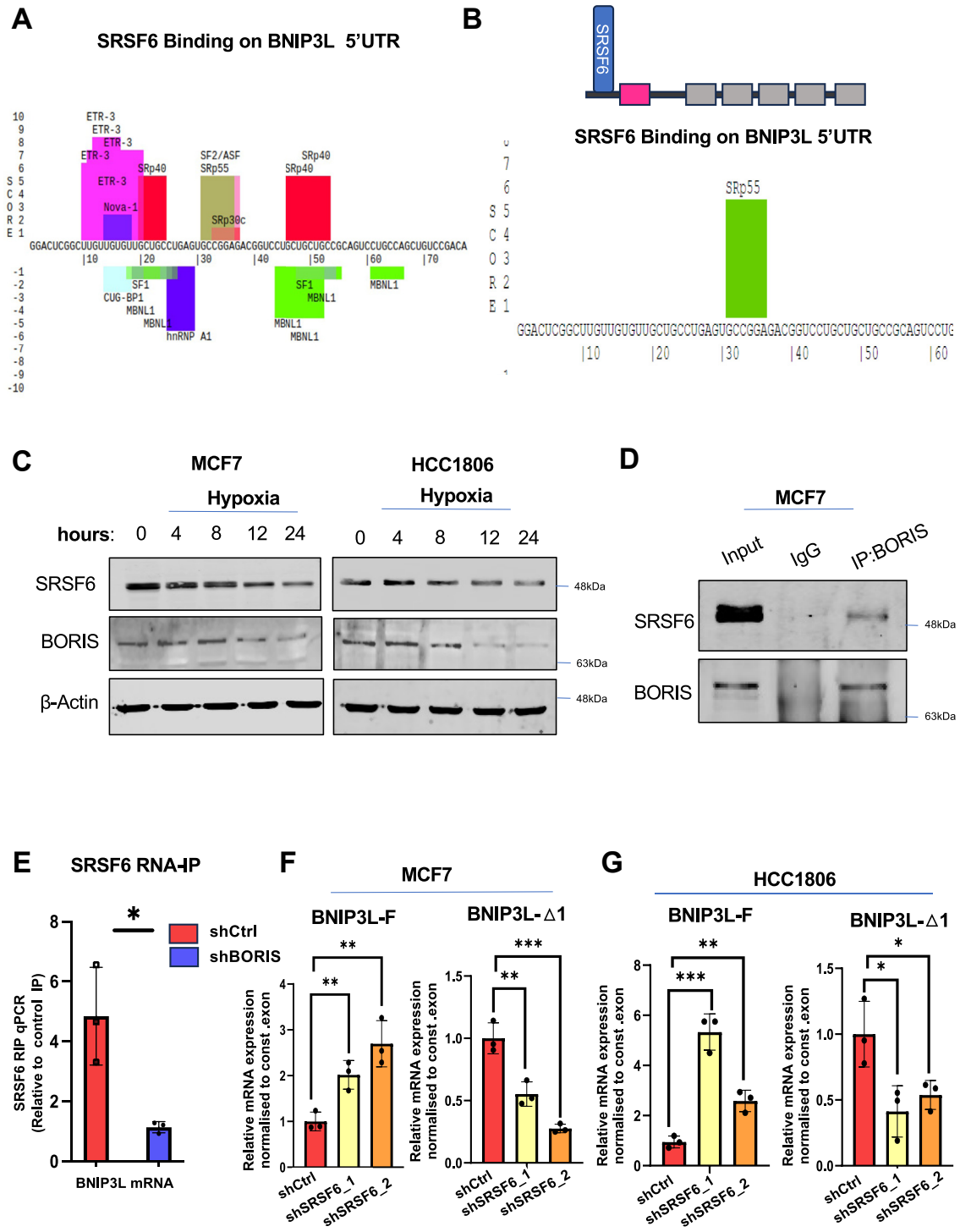


**Figure 5. BORIS recruits SRSF6, resulting in the exclusion of exon 1 in BNIP3L mRNA under normoxia.** *A*, SpliceAid tool indicating the binding of different splicing factors at BNIP3L 5′UTR. *B*, binding of SRSF6 at BNIP3L 5′UTR and a schematic indicating the same. *C*, immunoblot measuring SRSF6 and BORIS expression at different time points of hypoxic MCF7 and HCC1806 cells. *D*, coimmunoprecipitation performed to show the interaction of BORIS and SRSF6 in MCF7 cell lysate. Immunoprecipitation is measured by immunoblot analyses using anti-SRSF6, anti-BORIS antibodies. *E*, RNA-immunoprecipitation (RIP)-qPCR analysis of SRSF6 transcript in control *versus* BORIS knockdown MCF7 cells using BNIP3L primer. Fold enrichment (SRSF6/IgG) normalized to input. *F* and *G*, BNIP3L isoforms expression measured in SRSF6 knockdown (*F*) MCF7 and (*G*) HCC 1806 cell lines. Data represent the mean ± SD from three independent experiments. Statistical significance was determined using unpaired Student's t test (*$p < 0.05$, **$p < 0.01$, ***$p < 0.001$, and ****$p < 0.0001$, while a lack of significance is represented by "ns" for $p > 0.05$). Error bars show mean values ± SD (n = 3 unless otherwise specified).

broadened our study by examining the impact of BORIS on autophagy under hypoxia. We exogenously expressed Flag tag-BORIS under hypoxia. Intriguingly, when we exogenously expressed BORIS Flag-tag in breast cancer cells under hypoxia, the increase in LC3-GFP puncta and LC3B-II/LC3B-I ratio under hypoxia as compared to normoxia cells was subsequently decreased (Fig. 6, *F–H*). These results suggested that an increase in the expression of BORIS under hypoxia

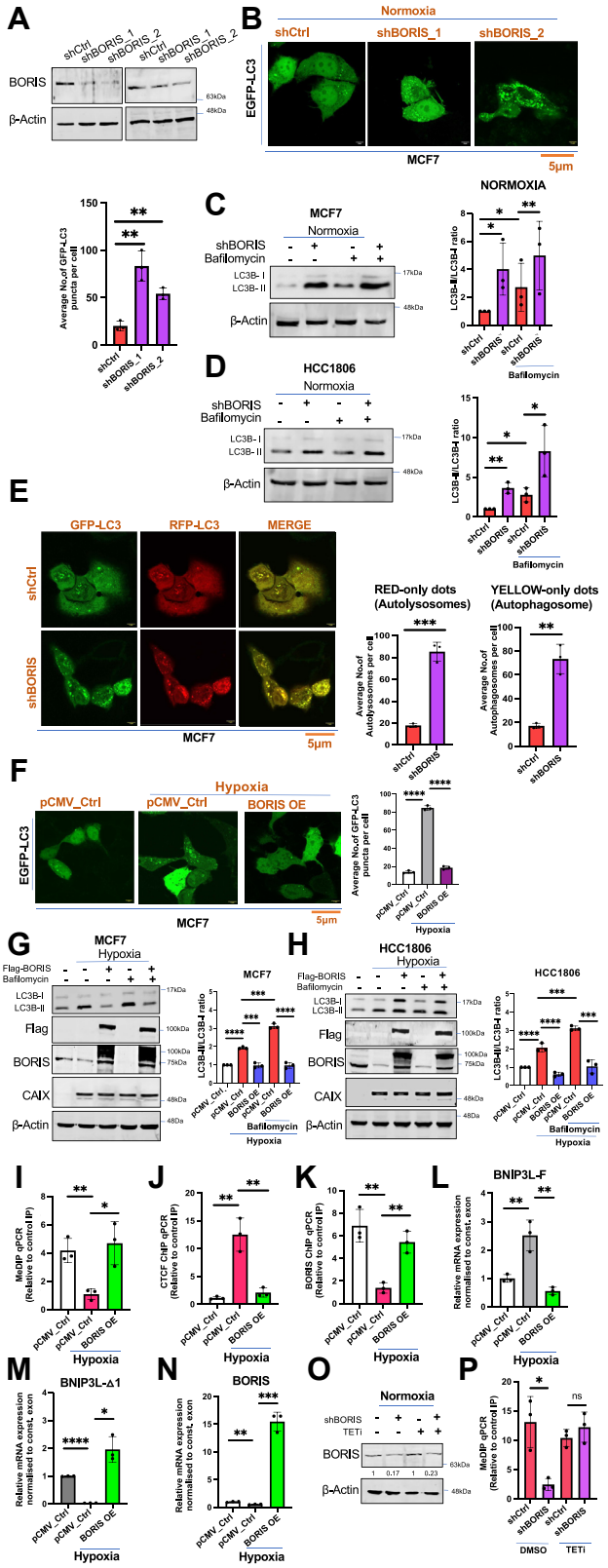


**Figure 6. BORIS inhibits hypoxia-induced autophagy.** *A*, immunoblots measuring BORIS expression in BORIS knockdown MCF7 and HCC1806 cells. *B*, BORIS knockdown MCF7 cells transfected with EGFP-LC3 plasmid. The scale bar represents 5 μm. Data represent the mean ± SD from three independent experiments. *C–D*, immunoblot measuring (*C*) LC3B-II/LC3B-I ratios in BORIS knockdown (*C*) MCF7 and (*D*) HCC 1806 cells, incubated in hypoxia for 12 h. The same cells were treated with Bafilomycin and were taken as a positive control. Graph showing the average of three independent experiments measuring LC3B-II/LC3B-I ratio. *E*, ptf-LC3 transfected in BORIS knockdown MCF7 cells. The scale bar represents 5 μm. Data represent the mean ± SD from three independent experiments. The average number of autophagosomes (*yellow only dots*) and autolysosome puncta (*red only dots*) was analyzed in three independent experiments. *F*, exogenously expressed BORIS in MCF7 cells were transfected with EGFP-LC3 plasmid, and cells were incubated in hypoxia (1% oxygen) for 12 h. LC3–GFP puncta were analyzed. The scale bar represents 5 μm. Data represent the mean ± SD from three independent experiments. *G* and *H*, immunoblots measuring LC3B-II/LC3B-I ratio in exogenously expressed BORIS (*G*) MCF7 cells and (*H*) HCC1806 cells. Graph showing the average of three independent experiments measuring LC3B-II/LC3B-I ratio. *I*, MeDIP performed in exogenously expressed BORIS in MCF7 cells at BNIP3L intron 1 incubated in hypoxia for 12 h. *J* and *K*, ChIP of (*J*) CTCF and (*K*) BORIS performed in exogenously expressed BORIS in MCF7 cells at BNIP3L intron 1 incubated in hypoxia for 12 h. *L–N*, BNIP3L isoform expression measured by qPCR performed in exogenously expressed BORIS in hypoxic (12 h) MCF7 cells. *O*, immunoblot measuring BORIS expression in DMSO *versus* ten eleven translocases inhibitor (TETi) (bobcat) treated BORIS knockdown MCF7 cells. *P*, MeDIP perfomed in DMSO *versus* TETi (bobcat) treated BORIS knockdown cells at BNIP3L intron 1. Data represent the mean ± SD from three independent experiments. Statistical significance was determined using unpaired Student's t test (*$p < 0.05$, **$p < 0.01$, ***$p < 0.001$, and ****$p < 0.0001$, while a lack of significance is represented by "ns" for $p > 0.05$). Error bars show mean values ± SD (n = 3 unless otherwise specified). ChIP, chromatin immunoprecipitation; DMSO, dimethyl sulfoxide; MeDIP, methylated DNA immunoprecipitation; qPCR, quantitative PCR.

abolished autophagosome formation. So, we next asked whether BORIS-associated methylation under hypoxia affects CTCF binding on BNIP3L intron 1. We examined the methylation level using MeDIP-qPCR in BORIS overexpressed cells as compared to control hypoxic and normoxic cells. We observed that the decrease in methylation of BNIP3L intron 1 from normoxic to hypoxic condition was rescued by exogenously expressing Flag tag-BORIS under hypoxic condition (Fig. 6*I*). Furthermore, BORIS-associated methylation under hypoxia resulted in a decrease in the enrichment of CTCF on BNIP3L intron 1 in BORIS overexpressed cells as compared to control hypoxic cells (Fig. 6, *J* and *K*). More importantly, our qRT-PCR analyses also showed a decrease in BNIP3L-F and an increase in BNIP3L-△1 expression in cells with exogenously expressed Flag-tag BORIS under hypoxia (Fig. 6L-N) that aligns with the data as illustrated in (Fig. 3, *G* and *H*).

Since active DNA demethylation of the gene is achieved through ten-eleven translocases (TETs) that are responsible for oxidation of 5-mC to 5-hmC (16). We next questioned the mechanism of DNA demethylation of BNIP3L intron 1 in BORIS-depleted cells. We performed MeDIP-qPCR in control *versus* BORIS-depleted cells while inhibiting TETs using Bobcat (TET inhibitor). We discovered that TET inhibition restored methylation at BNIP3L intron 1 in BORIS-depleted cells. This observation indicates that depletion of BORIS expression under hypoxia is vital for TETs in DNA demethylation of BNIP3L intron 1 (Fig. 6, *O–P*).

These results demonstrate the hypoxia-mediated interplay between CTCF and BORIS in the regulation of autophagy. Additionally, it indicates that BORIS-associated methylation under hypoxia impedes CTCF binding and autophagy induction.

## Discussion

Autophagy is a self-regulatory catabolic process that plays a crucial role in maintaining cellular integrity and eradicating

toxic molecules (29). The proliferative cancer cells ensure sustenance within tumor mass by continuously adapting to stressful conditions. Indeed, cancer cells utilize autophagy as a tool to sustain robust responses, fulfilling energy requirements, and escaping stressful conditions (30, 31). The complexity and versatility displayed by autophagy allow it to be regulated by a plethora of stimuli, including hypoxia (11, 32). Thereby, it becomes compelling to comprehend the complex regulatory autophagic network during tumor progression.

Recently, González *et al.* have summarized the role of alternative splicing and generation of autophagy-related isoforms in the regulation of autophagy (33). However, whether alternative splicing participates in regulating autophagic genes in the hypoxic landscape of tumor is still elusive. Here in our study, we discovered hitherto unreported hypoxia-dependent alternative splicing of BNIP3L, a hypoxia-driven autophagic gene (34), in breast cancer cells. We showed that BNIP3L mRNA produces two isoforms, each with a functional relevance for autophagy. Previously, the role of BNIP3L has been widely studied in mitophagy and various diseases such as ischemia and schizophrenia (23). However, considering the multifaceted role of autophagy during cancer progression (9), it becomes important to comprehend the role of two isoforms of BNIP3L in regulating autophagy in breast cancer cells. The two isoforms include a longer functional isoform (BNIP3L-F) that contains exon 1 and promotes autophagy (Fig. 2, *G* and *H*). Exon 1 encodes the LIR domain, which is essential for recruiting autophagosomes and induction of autophagy (22, 23, 35). Whereas the other shorter isoform (BNIP3L-Δ1) lacks exon 1 and inhibits autophagy. We showed that the two isoforms formed by exon 1 skipping of BNIP3L mRNA also differ in their potential interaction with Bcl-2 to dissociate the Bcl-2-BECN1 complex that affects autophagy. Our study showed the interaction of BNIP3L-F with Bcl-2 relative to BNIP3L-Δ1 (Fig. 2, *I–K*). Thereby, we can conclude that better interaction of BNIP3L-F with Bcl-2 disrupts the Bcl-2-BECN1 complex that promotes autophagy.

Epigenetics encompasses the biochemical alteration of chromatin that controls gene expression without changing DNA sequences (36). The most recognized epigenetic modifications, such as DNA methylation, noncoding RNA, and histone modifications, alter DNA accessibility and chromatin structure (37, 38). Several genes in the realm of autophagy have been shown to be regulated by DNA methylation in various cancers. In breast cancer, BECN1 gets frequently inactivated due to the loss of heterozygosity and hypermethylation at the promoter (39). Hypermethylation of BNIP3 has also been reported in colorectal carcinoma (40). Several other genes, including ATG4D, ATG9A, and GABARAPL1, have hypermethylation at promoters, affecting their gene expression (41, 42). Additionally, DNA methylation also seems highly responsible for changes in the chromatin organization and recruitment of selective DNA binding proteins (43). The unique zinc finger paralogous DNA/RNA binding protein pair CTCF and BORIS bind DNA sequences in DNA methylation-dependent specificity and affect the transcription of several genes (44). The methylation-sensitive binding of CTCF has provided insights into putative mechanisms in regulating gene expression and alternative splicing of various genes (44).

Here, our study delineates the role of CTCF in regulating autophagy under hypoxia. Evidently, CTCF under hypoxia promotes autophagy by regulating autophagosome formation. Additionally, we also identified the unique binding site of CTCF on BNIP3L intron 1 that causes RNA Pol II pause and promotes BNIP3L alternative splicing. The binding of CTCF on unmethylated DNA sequences at intron 1 under hypoxia resulted in stalling RNA Pol II and subsequent selection of weak proximal splice sites that promoted the exon 1 retention (BNIP3L-F) (Fig. 7).

BORIS, also called CTCFL protein, shows remarkably extensive homology with the central 11-zinc finger region of CTCF but not the N- and C-terminal region. Although CTCF and BORIS share the same site-specific DNA binding domain (26), the impact of BORIS binding cannot mediate the same effects as CTCF upon interaction with DNA. BORIS has been previously identified for its potential binding on methylated DNA sequences and regulating alternative splicing by alternate exon retention (14). In this study, we showed that BORIS inhibits autophagy by inhibiting autophagosome formation. Here, we untangled a novel regulatory mechanism of BORIS-mediated alternative splicing of autophagic gene that resulted in the exclusion of exon 1 under normoxia. These observations suggested another peculiarity of BORIS, where we also highlighted the role of BORIS in recruiting a splicing factor, SRSF6. The recruitment of SRSF6 with the aid of BORIS redirected the splice site selection, causing the exclusion of exon 1 forming BNIP3L-Δ1 (Fig. 7). Although, it is promising that CTCF and BORIS regulates autophagy in breast cancer, further investigations are still needed to ascertain the impact of CTCF and BORIS mediated autophagy on tumor progression.

Furthermore, our data clearly showed that the repression of BORIS under normoxia coincides with the demethylation of intron 1 followed by an increase in occupancy of CTCF under normoxia and the formation of BNIP3L-F isoform promoting autophagy. We further corroborated that the knockdown of BORIS under normoxia is essential for the TETs accounting for the DNA demethylation (Fig. 6*P*). However, the precise mechanism behind BORIS-associated methylation still needs further investigation. These findings untangled the mechanism of inhibition of autophagy by BORIS and promoting BNIP3L-Δ1 under normoxia. Taken together, our study unveils the interesting hypoxia-driven differential DNA methylation and interplay of CTCF and BORIS binding, with an involvement of SRSF6 in alternative splicing of BNIP3L, which regulates hypoxia-induced autophagy.

Hypoxia-induced autophagy is a dynamic process, and the aberrant alternative splicing of autophagy-regulating genes provides initial insights into a complex regulatory network of autophagy in the cancer milieu. Our study uncovered the alternative splicing of BNIP3L that can be selectively exploited for targeting autophagy and to study the repercussions of breast cancer progression connected with it. Taking into account the contribution of autophagy in chemotherapy

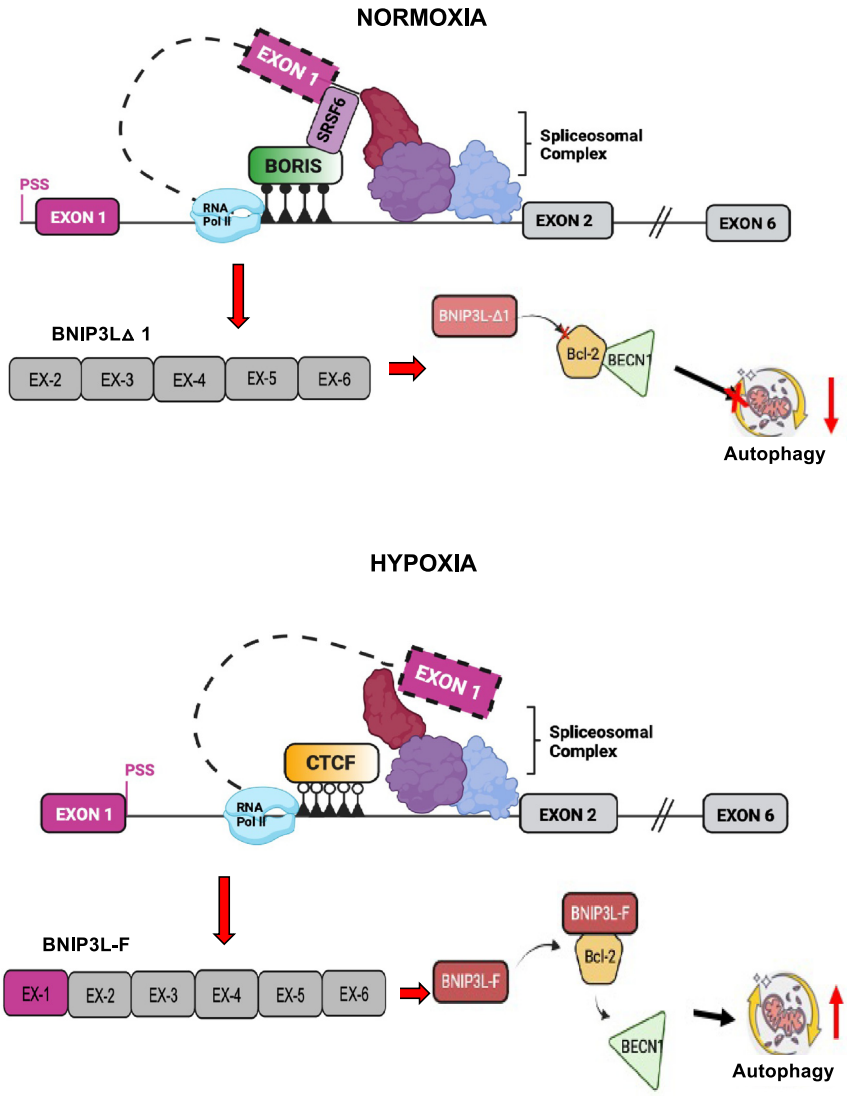


**Figure 7. Graphical abstract.** Figure showing the binding of BORIS on methylated BNIP3L intron 1 interacting with SRSF6 that results in BNIP3L-△1 isoform inhibiting autophagy under normoxia. CTCF binding on unmethylated BNIP3L intron 1 under hypoxia promoting BNIP3L-F and autophagy.

resistance, this study provides new insights into autophagy-related cancer therapeutics.

## Experimental procedures

### *Cell culture and treatment*

Breast cancer MCF7 (non-TNBC), HCC1806 (TNBC), and HEK293T cell lines were obtained from the American Type Culture Collection and were maintained in the American Type Culture Collection recommended medium. MCF7 and HEK293T were grown in Dulbecco's modified Eagle's medium, and HCC1806 was grown in RPMI-1640. Both the mediums were supplemented with 10% fetal bovine serum (FBS; Sigma-Aldrich, F7524), 100 units/ml of penicillin and streptomycin (Invitrogen, 15140122), and 2 mmol/l L-glutamine (Sigma-Aldrich, G7513). All cell lines were cultured in a humidified atmosphere at 37 °C and 5% CO2. The hypoxic treatment (1% $O_2$) (6, 45) to the cells was given in Ruskinn InvivO2 400 hypoxia chamber for different time points (0, 4, 8, 12, and 24 h). The 0.3 μM of bafilomycin treatment was given to cells prior 3 h before harvesting. The cell lines used in the study were authenticated from a national cell repository facility by short tandem repeats profiling and were routinely tested for *mycoplasma* contamination using a PCR-based method.

### *qRT-PCR*

Total RNA was extracted from breast cancer cells using TRIzol reagent (Invitrogen, Cat# 15596018, lot no. 260712) according to the manufacturer's instructions. The RNA was quantified using Nanodrop (Thermo Fisher Scientific, ND8000). Total RNA (2 μg) was then reverse-transcribed with PrimeScript 1st strand DNA synthesis kit (Takara, Cat# 6110A) as per the manufacturer's instructions. A total of 20 ng of complementay DNA (cDNA) was used as the template for PCR amplification. RT-PCR products were separated on 2%

gels. The amplification of the samples was performed using SYBR Green (Promega A6002, lot no. 0000385100) and qTOWER3G (Analytik Jena) according to the manufacturer's protocol. The primers were designed using the Integrated DNA Technologies PrimerQuest tool (Table S1). The average cycle threshold of three independent replicates was calculated, and for normalization of the assay, the housekeeping gene RPS16 was used in the following formula: 2^ (Ct control—Ct target). Additionally, for individual exon-level expressions, each was normalized to a constitutive exon. To validate and compare gene/exon expression between two individual groups, student's *t* test was performed. *p*-Value less than 0.05 was considered as statistically significant.

### Semiquantitative PCR

After obtaining cDNA as mentioned earlier, amplification of DNA was performed using DreamTaq polymerase (Thermo Fisher Scientific, EP0702) in PCR reactions. The specific primers, including exon junction primers, were designed by using the Integrated DNA Technologies PrimerQuest tool and are mentioned in Table S1. PCR products were analyzed on a 2% agarose gel after ethidium bromide staining.

### Western blot

Cells were harvested with radioimmunoprecipitation assay lysis buffer containing (20 mM Tris pH 8.0; 1 mM EDTA; 0.5 mM EGTA; 0.1% sodium deoxycholate; 150 mM NaCl; 1% IGEPAL; and 10% glycerol) (46) with protease inhibitor cocktail (leupeptin 0.5 mM, pepstatin 1 μM, and 50 mM EDTA), and 1 mM PMSF. Cell debris was removed by centrifugation, and protein samples (30 μg) were boiled for 5 min in 1× SDS sample buffer. The protein samples were fractionated using 15% SDS-PAGE and transferred to the polyvinylidene fluoride membrane. The membrane was blocked by 10% skimmed milk for 1 h and incubated with antibodies overnight at 4 °C. After washing thrice for 5 min each, the membrane was incubated for 1 h in secondary antibody at room temperature. The bands were quantified using Fiji Image J software (https://fiji.sc), and the LC3B-II/LC3B-I ratio was calculated by taking an average of three independent experiments. The antibodies used are mentioned in Table S4.

### Fluorescence microscopy analysis

For monitoring autophagy, in a 12-well plate, approximately $10^5$ cells were seeded on a coverslip and allowed to adhere to the surface with 70% confluency. These cells were then transfected with 2 μg of reporter plasmid (EGFP-LC3 #Addgene 11546) using lipofectamine 2000 for 12 h and then kept in a hypoxic chamber for 12 h. The adhered cells, after 3× cold PBS washes, were fixed in 4% paraformaldehyde for 15 min and visualized using Leica (TCS SP5×) in a confocal microscope with an ×60 oil objective. The number of GFP-LC3 puncta per cell was analyzed and quantified using Fiji ImageJ software.

The same cells were transfected with ptf-LC3 reporter plasmid (EGFP-mRFP-LC3 # Addgene 21074) using lipofectamine 2000. The images were obtained from Leica (TCS SP5×) in a confocal microscope with a ×60 oil objective. Autophagosomes were detected as $GFP^+$ $RFP^+$ (yellow only dots) and mature autolysosomes as $GFP^-$ $RFP^+$ (red only dots). The number of puncta per cell was analyzed and quantified using Fiji ImageJ software (https://fiji.sc).

### Coimmunoprecipitation

The interaction of BNIP3L isoforms and BECN1 with Bcl-2 and BORIS-SRSF6 was evaluated by performing Co-IP, as done previously. Flag-tag BNIP3L-F and BNIP3L-Δ1 overexpression constructs were transfected using lipofectamine 2000 in BNIP3L knockdown cells. These cells were washed with ice-cold PBS and were lysed using a 1% NP40 lysis buffer [50 mM Tris, 150 mM NaCl, 1 mM EDTA, 1% NP-40, and 10% glycerol] and protease inhibitor cocktail (leupeptin 0.5 mM, pepstatin 1 μM, 50 mM EDTA), and 1 mM PMSF. Equal concentrations of the lysate were divided for incubation with 2 μg of anti-FLAG antibody, anti-BECN1, anti-BORIS, or anti-Bcl-2 antibody along with normal rabbit immunoglobulin G (IgG) for 8 h at 4 °C with constant rotation. Subsequently, for input 5% aliquot of the supernatant was kept separately. Followed by pulling down the desired protein by incubating the immunoprecipitated lysate with 20 μl of Protein-G Dynabeads (Thermo Fisher Scientific, 10004D, lot 0078227) for the next 2 h at 4 °C. The lysates were removed, and the beads were washed thrice with the NP40 lysis buffer. The beads were then eluted in 30 μl of 2× Laemmli buffer and boiled for 5 min at 95 °C. Immunoblotting analysis was performed with the eluted proteins with anti-FLAG, anti-BECN1, anti-BNIP3L, anti-Bcl-2, anti-CTCF, anti-BORIS, and anti-SRSF6 antibodies (Table S4).

### RNA immunoprecipitation

The recruitment of SRSF6 by BORIS was deciphered by performing RNA-IP of SRSF6 in control *versus* BORIS knockdown MCF7 cells. The RNA-IP assay was performed as described previously (45). The control and knockdown cells were seeded in a 100 mm dish, after reaching 80% confluency, the cells were washed twice with 1 ml ice-cold PBS and incubated 5 min for lysis with 1.5 ml of ice-cold swelling buffer A (25 mM Hepes, 1.5 mM MgCl2, and 85 mM KCl, pH 8.0). The cells were scraped, followed by centrifugation at 1350*g* for 10 min at 4 °C, the collected pellet was resuspended with 1 ml of buffer C (25 mM Hepes, 1.5 mM $MgCl_2$, 85 mM KCl, pH 8.0, 0.2% NP-40, 1% Triton X-100, 1× PIC, 2U/ml of RNaseOUT, 5 mM sodium fluoride, 5 mM sodium orthovanadate, and 5mM-glycerophosphate) and kept for lysis with perpetual rotation at 4 °C for 30 min. The lysate was split into two fractions of 500 μl each for IgG and IP. Subsequently, for input 5% aliquot of the supernatant was kept separately. Subsequently, 3 μg of anti-SRSF6 was added to the IP supernatant and incubated for 5 h at 4 °C with gentle rotation. Afterward, 20 μl of Dynabeads was added to each sample and incubated for the next 2 h at 4 °C with gentle rotation. The beads were washed thrice for 5 min each with 500 μl of buffer D (25 mM Hepes, 1.5 mM MgCl2, 85 mM KCl, pH 8.0, 0.02% NP-40, 0.25% Triton X-100, 1 × PIC, 0.1 U/ml of RNaseOUT,

5 mM sodium fluoride, 5 mM sodium orthovanadate, and 5mM-glycerophosphate). The beads were resuspended in TRIzol RNA extraction reagent (Invitrogen, 15596026), and RNA was isolated according to the manufacturer's instructions. cDNA was synthesized using total RNA isolated by PrimeScript 1st strand cDNA Synthesis Kit (TaKaRa, 6110 A, lot no. AJX1015N) as per the manufacturer's instructions.

### Chromatin immunoprecipitation

The occupancy of CTCF, RNA Pol II, and BORIS on their respective binding sites on the BNIP3L gene was determined using ChIP-qPCR as described previously (45). Initially, normoxia *versus* hypoxia treated MCF7 cells in 150 mm dishes were lysed and sonicated to generate chromatin fragments of lengths ranging from 100 to 300 bp. A total of 25 μg of sonicated chromatin was incubated overnight at 4 °C with 3 μg of concomitant antibodies. The immunoprecipitated lysate was incubated with 20 μl of magnetic beads and incubated at 4 °C for the next 2 h. The magnetic beads were further washed with low salt, high salt, LiCl, and Tris-EDTA buffer. The immunoprecipitated protein–DNA complexes and 5% input were analyzed in triplicate by qRT-PCR with SYBR Green master mix (Promega A6002, lot no. 0000385100) using specific primers flanking the predicted binding sites (Table S2). IP values were normalized to input using the following formula: 2^ (Ct input−Ct immunoprecipitation). Resultant values were normalized to IgG control IP values. All the ChIP experiments were performed at least thrice. The significance between different groups was determined using a Student's *t* test, with a *p*-value less than 0.05 considered statistically significant. The following antibodies were used: anti-CTCF, anti-BORIS, anti-CTD, normal rabbit IgG, and normal mouse IgG (Table S4).

### Methylated DNA immunoprecipitation

The genomic DNA of normoxia and hypoxia-treated MCF7 and HCC1806 cells was extracted using the genomic DNA isolation kit (Sigma-Aldrich G1N350) according to the manufacturer's instructions. Genomic DNA was sonicated to get DNA fragments between 250 to 500 bp size and was denatured by incubating at 95 °C for 10 min Subsequently, 3 μg of sonicated DNA was incubated with 1 μg anti-5-methylcytosine antibodies along with normal rabbit IgG at 4 °C overnight. The immunoprecipitated lysate with 20 μl of magnetic beads was incubated for the next 2 h at 4 °C. The beads were washed thrice with 500 μl MeDIP buffer at 4 °C for 5 min and eluted in 150 μl elution buffer with proteinase K treatment overnight at 65 °C. PCR purification was performed using a Qiagen PCR purification kit. The immunoprecipitated fractions and 5% input were analyzed using quantitative real-time PCR using the SYBR Green Master Mix (Promega, A6002, lot no. 0000385100) and specific primers (Table S2). The experiments were performed at least in triplicate. IP values were normalized to input using the formula: 2^ (Ct_input−Ct_immunoprecipitation). The significance between the two different groups was determined using a Student's *t* test, with a *p*-value of less than 0.05 considered statistically significant.

### RNA interference

To stably produce knockdown of BORIS, BNIP3L, CTCF, and SRSF6 in MCF7 and HCC1806 cells, lentiviral vectors were used. We transfected HEK293T cells with shRNA against BORIS, BNIP3L, CTCF, and SRSF6 along with the Δ8.9 and VSVG plasmid in the ratio 2:1:0.5 using PEI to generate the lentivirus containing specific shRNA plasmid. The supernatants containing lentivirus were collected, followed by centrifugation to remove any cellular contaminant. Consequently, MCF7 and HCC1806 cells were infected with the prepared lentiviral particles, and the stably integrated cells were selected with 0.8 μg/ml puromycin for 3 days. Then, the cells were maintained in a medium containing 1 μg/ml puromycin at 37 °C in a humidified incubator with 5% $CO_2$. All the stable cell lines were confirmed by Western bolts and qRT-PCR before for further analysis. The shRNAs are provided in the Table S3.

### Molecular cloning

The overexpression construct for BORIS, BNIP3L -F, and BNIP3L-Δ1 isoforms were prepared using pCMV-3Tag-1a overexpression plasmid Agilent (240195). The amplification was carried out using Phusion polymerase and hypoxia-treated MCF7 and HCC1806 cDNA using primers, as mentioned in Table S1. The amplified products were inserted between EcoRI forward and HindIII reverse sites of the plasmid for BNIP3L and between EcoRI forward and SalI reverse sites for BORIS. The overexpressed clones were confirmed in Western blotting against anti-FLAG.

### The binding of CTCF on BNIP3L intron 1

CTCF binding on BNIP3L intron 1 was analyzed in ChIP-Atlas peak browser in breast cancer cell lines.

### Quantification and statistical analysis

LC3-GFP, LC3-GFP-RFP, and LC3-RFP puncta were quantified using Fiji imageJ software. All statistical analyses were conducted using GraphPad Prism 9 software (GraphPad Software https://www.graphpad.com/scientificsoftware/prism/). Unless otherwise stated, all data are represented as mean ± SD analyzed using an unpaired two-tailed Student's *t* test. Statistical methods for each analysis are described in figure legends. Independently performed biological replicates are indicated as dots in the bar graphs. Statistical significance is denoted as follows: $^{*}p < 0.05$, $^{**}p < 0.01$, $^{***}p < 0.001$, and $^{****}p < 0.0001$, while a lack of significance is represented by "ns" for $p > 0.05$.

## Data availability

The data that support the findings of this study are available within the article.

*Supporting information*—This article contains supporting information.

*Acknowledgments*—The authors express their gratitude to all the members of Epigenetics and RNA processing lab. This research was

funded by Ministry of Education, Scheme for Transformational and Advanced Research in Sciences (STARS) (MoE-STARS/STARS-2/2023-0843). This project is also supported by Science and Engineering Research Board (SERB) Grant (CRG/2021/004949, STR/2020/000093, and IPA/2021/000148).

*Author contributions*—A. P., P. K., and S. S. writing–review and editing; A. P., P. K. and S. S. formal analysis; A. P. and S. S. conceptualization; A. P. and S. S. investigation; A. P. and S. S. writing–original draft; A. P. data curation; A. P. methodology; A. P. validation; S. S. project administration; S. S. supervision; S. S. resources; S. S. funding acquisition.

*Funding and additional information*—The work was supported by the Prime Minister Research Fellowship (to A. P.).

*Conflict of interest*—The authors declare that they have no conflicts of interest with the contents of this article.

*Abbreviations*—The abbreviations used are: cDNA, complementary DNA; ChIP, chromatin immunoprecipitation; Co-IP, coimmunoprecipitation; CTCF, CCCTC-binding factor; EGFP, Enhanced GFP; IgG, immunoglobulin G; IP, immunoprecipitation; MeDIP, methylated DNA immunoprecipitation; qPCR, quantitative PCR; qRT-PCR, quantitative reverse transcription PCR; LC3B, microtubule associated protein 1A/1B light chain 3B; TET, ten-eleven translocase.

## References


1. Chen, A., Sceneay, J., Gödde, N., Kinwel, T., Ham, S., Thompson, E. W., *et al.* (2018) Intermittent hypoxia induces a metastatic phenotype in breast cancer. *Oncogene* **37**, 4214–4225
2. Hanahan, D. (2022) Hallmarks of cancer: new dimensions. *Cancer Discov.* **12**, 31–46
3. Ye, L. Y., Chen, W., Bai, X. L., Xu, X. Y., Zhang, Q., Xia, X. F., *et al.* (2016) Hypoxia-induced epithelial-to-mesenchymal transition in hepatocellular carcinoma induces an immunosuppressive tumor microenvironment to promote metastasis. *Cancer Res.* **76**, 818–830
4. Narod, S. A., and Sopik, V. (2018) Is invasion a necessary step for metastases in breast cancer? *Breast Cancer Res. Treat* **169**, 9–23
5. Wang, C., Jiang, J., Ji, J., Cai, Q., Chen, X., Yu, Y., *et al.* (2017) PKM2 promotes cell migration and inhibits autophagy by mediating PI3K/AKT activation and contributes to the malignant development of gastric cancer. *Sci. Rep.* **7**, 2886
6. Yadav, P., Pandey, A., Kakani, P., Mutnuru, S. A., Samaiya, A., Mishra, J., *et al.* (2023) Hypoxia-induced loss of SRSF2-dependent DNA methylation promotes CTCF-mediated alternative splicing of VEGFA in breast cancer. *iScience* **26**, 106804
7. Bellot, G., Garcia-Medina, R., Gounon, P., Chiche, J., Roux, D., Pouysségur, J., *et al.* (2009) Hypoxia-induced autophagy is mediated through hypoxia-inducible factor induction of BNIP3 and BNIP3L via their BH3 domains. *Mol. Cell Biol.* **29**, 2570–2581
8. Marsh, T., and Debnath, J. (2020) Autophagy suppresses breast cancer metastasis by degrading NBR1. *Autophagy* **16**, 1164–1165
9. Russell, R. C., and Guan, K.-L. (2022) The multifaceted role of autophagy in cancer. *EMBO J.* **41**, e110031
10. Hu, Y.-L., DeLay, M., Jahangiri, A., Molinaro, A. M., Rose, S. D., Carbonell, W. S., *et al.* (2012) Hypoxia-induced autophagy promotes tumor cell survival and adaptation to antiangiogenic treatment in glioblastoma. *Cancer Res.* **72**, 1773–1783
11. Qureshi-Baig, K., Kuhn, D., Viry, E., Pozdeev, V. I., Schmitz, M., Rodriguez, F., *et al.* (2020) Hypoxia-induced autophagy drives colorectal cancer initiation and progression by activating the PRKC/PKC-EZR (ezrin) pathway. *Autophagy* **16**, 1436–1452
12. Maor, G. L., Yearim, A., and Ast, G. (2015) The alternative role of DNA methylation in splicing regulation. *Trends Genet.* **31**, 274–280
13. Debaugny, R. E., and Skok, J. A. (2020) CTCF and CTCFL in cancer. *Curr. Opin. Genet. Dev.* **61**, 44–52
14. Singh, S., Narayanan, S. P., Biswas, K., Gupta, A., Ahuja, N., Yadav, S., *et al.* (2017) Intragenic DNA methylation and BORIS-mediated cancer-specific splicing contribute to the Warburg effect. *Proc. Natl. Acad. Sci. U. S. A.* **114**, 11440–11445
15. Shukla, S., Kavak, E., Gregory, M., Imashimizu, M., Shutinoski, B., Kashlev, M., *et al.* (2011) CTCF-promoted RNA polymerase II pausing links DNA methylation to splicing. *Nature* **479**, 74–79
16. Marina, R. J., Sturgill, D., Bailly, M. A., Thenoz, M., Varma, G., Prigge, M. F., *et al.* (2016) TET-catalyzed oxidation of intragenic 5-methylcytosine regulates CTCF-dependent alternative splicing. *EMBO J.* **35**, 335–355
17. Klionsky, D. J., Abdel-Aziz, A. K., Abdelfatah, S., Abdellatif, M., Abdoli, A., Abel, S., *et al.* (2021) Guidelines for the use and interpretation of assays for monitoring autophagy (4th edition)[1]. *Autophagy* **17**, 1–382
18. Park, S. W., Kim, J., Oh, S., Lee, J., Cha, J., Lee, H. S., *et al.* (2022) PHF20 is crucial for epigenetic control of starvation-induced autophagy through enhancer activation. *Nucleic Acids Res.* **50**, 7856–7872
19. Zhang, G., Xu, Z., Yu, M., and Gao, H. (2022) Bcl-2 interacting protein 3 (BNIP3) promotes tumor growth in breast cancer under hypoxic conditions through an autophagy-dependent pathway. *Bioengineered* **13**, 6280–6292
20. Mauvezin, C., and Neufeld, T. P. (2015) Bafilomycin A1 disrupts autophagic flux by inhibiting both V-ATPase-dependent acidification and Ca-P60A/SERCA-dependent autophagosome-lysosome fusion. *Autophagy* **11**, 1437–1438
21. Liberzon, A., Birger, C., Thorvaldsdóttir, H., Ghandi, M., Mesirov, J. P., and Tamayo, P. (2015) The Molecular Signatures Database (MSigDB) hallmark gene set collection. *Cell Syst.* **1**, 417–425
22. Marinković, M., Šprung, M., and Novak, I. (2021) Dimerization of mitophagy receptor BNIP3L/NIX is essential for recruitment of autophagic machinery. *Autophagy* **17**, 1232–1243
23. Zhou, J., Ma, C., Wang, K., Li, X., Jian, X., Zhang, H., *et al.* (2020) Identification of rare and common variants in BNIP3L: a schizophrenia susceptibility gene. *Hum. Genomics* **14**, 16
24. Mellor, H. R., and Harris, A. L. (2007) The role of the hypoxia-inducible BH3-only proteins BNIP3 and BNIP3L in cancer. *Cancer Metastasis Rev.* **26**, 553
25. Bell, A. C., and Felsenfeld, G. (2000) Methylation of a CTCF-dependent boundary controls imprinted expression of the Igf2 gene. *Nature* **405**, 482–485
26. Hong, J. A., Kang, Y., Abdullaev, Z., Flanagan, P. T., Pack, S. D., Fischette, M. R., *et al.* (2005) Reciprocal binding of CTCF and BORIS to the NY-ESO-1 promoter coincides with derepression of this cancer-testis gene in lung cancer cells. *Cancer Res.* **65**, 7763–7774
27. de Oliveira Freitas Machado, C., Schafranek, M., Brüggemann, M., Hernández Cañás, M. C., Keller, M., Di Liddo, A., *et al.* (2023) Poison cassette exon splicing of SRSF6 regulates nuclear speckle dispersal and the response to hypoxia. *Nucleic Acids Res.* **51**, 870–890
28. Liang, L.-M., Xiong, L., Cheng, P.-P., Chen, S.-J., Feng, X., Zhou, Y.-Y., *et al.* (2020) Splicing factor SRSF6 mediates pleural fibrosis. *JCI Insight* **6**, e146197
29. Boya, P., Reggiori, F., and Codogno, P. (2013) Emerging regulation and functions of autophagy. *Nat. Cell Biol.* **15**, 713–720
30. Anderson, C. M., and Macleod, K. F. (2019) Autophagy and cancer cell metabolism. In *International Review of Cell and Molecular Biology* **347**. Elsevier: 145–190
31. Pandey, A., Yadav, P., and Shukla, S. (2021) Unfolding the role of autophagy in the cancer metabolism. *Biochem. Biophys. Rep.* **28**, 101158
32. Zhang, J., and Ney, P. A. (2009) Role of BNIP3 and NIX in cell death, autophagy, and mitophagy. *Cell Death Differ.* **16**, 939–946
33. González-Rodríguez, P., Klionsky, D. J., and Joseph, B. (2022) Autophagy regulation by RNA alternative splicing and implications in human diseases. *Nat. Commun.* **13**, 2735
34. Xu, Y., Shen, J., and Ran, Z. (2019) Emerging views of mitophagy in immunity and autoimmune diseases. *Autophagy* **16**, 3–17

35. Wirth, M., Zhang, W., Razi, M., Nyoni, L., Joshi, D., O'Reilly, N., *et al.* (2019) Molecular determinants regulating selective binding of autophagy adapters and receptors to ATG8 proteins. *Nat. Commun.* **10**, 2055
36. Li, Y. (2021) Modern epigenetics methods in biological research. *Methods* **187**, 104–113
37. Sharma, S., Kelly, T. K., and Jones, P. A. (2010) Epigenetics in cancer. *Carcinogenesis* **31**, 27–36
38. Narayanan, S. P., Singh, S., and Shukla, S. (2017) A saga of cancer epigenetics: linking epigenetics to alternative splicing. *Biochem. J.* **474**, 885–896
39. Li, Z., Chen, B., Wu, Y., Jin, F., Xia, Y., and Liu, X. (2010) Genetic and epigenetic silencing of the beclin 1 gene in sporadic breast tumors. *BMC Cancer* **10**, 98
40. Uetake, H., Iida, S., and Sugihara, K. (2008) Promoter hypermethylation of BNIP3 and prognosis in human colorectal cancer. *J. Clin. Oncol.* **26**, 15025
41. Khalil, H., Tazi, M., Caution, K., Ahmed, A., Kanneganti, A., Assani, K., *et al.* (2016) Aging is associated with hypermethylation of autophagy genes in macrophages. *Epigenetics* **11**, 381–388
42. Shu, F., Xiao, H., Li, Q.-N., Ren, X.-S., Liu, Z.-G., Hu, B.-W., *et al.* (2023) Epigenetic and post-translational modifications in autophagy: biological functions and therapeutic targets. *Sig Transduct Target Ther.* **8**, 1–23
43. Fournier, A., Sasai, N., Nakao, M., and Defossez, P.-A. (2012) The role of methyl-binding proteins in chromatin organization and epigenome maintenance. *Brief. Funct. Genomics.* **11**, 251–264
44. Alharbi, A. B., Schmitz, U., Bailey, C. G., and Rasko, J. E. J. (2021) CTCF as a regulator of alternative splicing: new tricks for an old player. *Nucleic Acids Res.* **49**, 7825–7838
45. Ahuja, N., Ashok, C., Natua, S., Pant, D., Cherian, A., Pandkar, M. R., *et al.* (2020) Hypoxia-induced TGF-β–RBFOX2–ESRP1 axis regulates human MENA alternative splicing and promotes EMT in breast cancer. *NAR Cancer.* **2**, zcaa021
46. Mehto, S., Jena, K. K., Nath, P., Chauhan, S., Kolapalli, S. P., Das, S. K., *et al.* (2019) The crohn's disease risk factor IRGM limits NLRP3 inflammasome activation by impeding its assembly and by mediating its selective autophagy. *Mol. Cell.* **73**, 429–445.e7